have played a role in the differentiation of Europa and Ganymede (*7*, *14*, *20*). The possibility that tidal heating due to Jupiter could have influenced the evolution of Ganymede, which is closer to Jupiter than Callisto, but not of the similarly large and massive Callisto is one way to reconcile the differentiation of Ganymede with the partial differentiation of Callisto (*6*).

REFERENCES AND NOTES

1. The first encounter (C3) occurred on 4 November 1996 at 11:47:09, the second (C9) occurred on 25 June 1997 at 13:47:50, and the third (C10) occurred on 17 September 1997 at 00:18:55, where the encounter times are expressed in Universal Time Coordinated (UTC) at the spacecraft, and the encounter designation Cn refers to an encounter with Callisto on the spacecraft's *n*th orbital revolution of Jupiter.
2. See, for example, T. D. Moyer, *Tech. Rep. No. TR 32-1527* (Jet Propulsion Laboratory, Pasadena, CA, 1971); B. D. Tapley, in *Recent Advances in Dynamical Astronomy*, B. D. Tapley and V. Szebehely, Eds. (Reidel, Dordrecht, Netherlands and Boston, MA, 1973), pp. 396–425; J. D. Anderson, in *Experimental Gravitation*, B. Bertotti, Ed. (Academic Press, New York, 1974), pp. 163–199.
3. W. M. Kaula, *Theory of Satellite Geodesy* (Blaisdell, Waltham, MA, 1966). The expression for V is

$$V(r,\phi,\lambda) = \frac{GM}{r}\left[1 + \sum_{n=2}^{\infty}\sum_{m=0}^{n}\left(\frac{R}{r}\right)^n \times (C_{nm}\cos m\lambda + S_{nm}\sin m\lambda)P_{nm}(\sin\phi)\right]$$

where M is the satellite's mass and G is the gravitational constant, $G = 6.6728 \pm 0.0016 \times 10^{-11}$ m^3 kg^{-1} s^{-2} [see E. R. Cohen and B. N. Taylor, *Phys. Today* **49**, BG9 (1996)]. The spherical coordinates (r, ϕ, λ) are referred to the center of mass, with r the radial distance, ϕ the latitude and λ the longitude on the equator. Callisto's reference radius R is 2403 km [see M. E. Davies *et al.*, *Celes. Mech.* **53**, 377 (1992)]. P_{nm} is the associated Legendre polynomial of degree n and order m, and C_{nm} and S_{nm} are the corresponding coefficients determined from the data.
4. W. B. Hubbard and J. D. Anderson, *Icarus* **33**, 336 (1978); S. F. Dermott, *ibid.* **37**, 310 (1979); V. N. Zharkov, V. V. Leontjev, A. V. Kozenko, *ibid.* **61**, 92 (1985); S. Mueller and W. B. McKinnon, *ibid.* **76**, 437 (1988); G. Schubert, D. Limonadi, J. D. Anderson, J. K. Campbell, G. Giampieri, *ibid.* **111**, 433 (1994).
5. Our adopted solution for Callisto's gravitational field fits the C9 and C10 Doppler data to within the noise level, but there is a residual signal at about the 3 mm s^{-1} level in the fit to the C3 data. This signal, of unknown origin, explains the difference between the C_{22} values from the independent fits for C3 and C10 (Table 1). Because the C9 data can be fit with the adopted gravitational field, the differences between the C9 and C10 independent fits are reconciled. We attribute the larger value of C_{22} from the independent C3 fit to systematic error in the noncoherent data, but we are not able to rule out completely the possibility that C3 is right and our adopted solution is wrong.
6. J. D. Anderson, E. L. Lau, W. L. Sjogren, G. Schubert, W. B. Moore, *Nature* **387**, 264 (1997).
7. Undifferentiated models of Callisto involve transformations of ice to phases such as ice II, ice VI, and ice VIII at depth in the satellite [M. J. Lupo, *Icarus* **52**, 40 (1982); J. Leliwa-Kopystynski, L. Makkonen, O. Erikoinen, K. J. Kossacki, *Planet. Space Sci.* **42**, 545 (1994)]. Other phases of ice (ice III and ice V) may occur depending on the radial profiles of temperature and pressure in the model interiors. The depths of the ice phase changes also depend on the temperature and pressure profiles [G. Schubert, D. J. Stevenson, K. Ellsworth, *Icarus* **47**, 46 (1981); G. Schubert, T. Spohn, R. T. Reynolds, in *Satellites*, J. A. Burns and M. S. Matthews, Eds. (Univ. of Arizona Press, Tucson, AZ, 1986), pp. 629–688].
8. W. B. McKinnon, *Icarus* **130**, 540 (1997).
9. P. V. Hobbs, *Ice Physics* (Clarendon Press, Oxford, 1974).
10. J. D. Anderson, E. L. Lau, W. L. Sjogren, G. Schubert, W. B. Moore, *Nature* **384**, 541 (1996).
11. A. J. Friedson and D. J. Stevenson, *Icarus* **56**, 1 (1983).
12. K. K. Khurana, M. G. Kivelson, C. T. Russell, R. J. Walker, D. J. Southwood, *Nature* **387**, 262 (1997).
13. J. Klemaszewski, personal communication.
14. G. Schubert, K. Zhang, M. G. Kivelson, J. D. Anderson, *Nature* **384**, 544 (1996).
15. S. W. Squyres and S. K. Croft, in *Satellites*, J. A. Burns and M. S. Matthews, Eds. (Univ. of Arizona Press, Tucson, AZ, 1986) pp. 293–341; W. B. McKinnon and E. M. Parmentier, in *Satellites*, J. A. Burns and M. S. Matthews, Eds. (Univ. of Arizona Press, Tucson, AZ, 1986) pp. 718–763; R. T. Pappalardo *et al.*, in preparation; G. C. Collins, J. W. Head, R. T. Pappalardo, *Geophys. Res. Lett.* **25**, 233 (1998); L. M. Prockter *et al.*, in preparation.
16. P. M. Schenk, *J. Geophys. Res.* **100**, 19023 (1995).
17. J. H. Lieske, *Astron. Astrophys.* **82**, 340 (1980).
18. S. J. Peale, P. Cassen, R. T. Reynolds, *Science* **203**, 892 (1979); M. Segatz, T. Spohn, M. N. Ross, G. Schubert, *Icarus* **75**, 187 (1988); M. N. Ross and G. Schubert, *ibid.* **64**, 391 (1985).
19. L. Keszthelyi and A. McEwen, *Icarus*, in press; A. S. McEwen *et al.*, in preparation.
20. R. Malhotra, *Icarus* **94**, 399 (1991); A. P. Showman and R. Malhotra, *ibid.* **127**, 93 (1997); A. P. Showman, D. J. Stevenson, R. Malhotra, *ibid.* **129**, 367 (1997).
21. R. Woo and J. W. Armstrong, *J. Geophys. Res.* **84**, 7288 (1979).

22. We thank the referee, W. B. McKinnon, for a careful review of the manuscript and for several suggestions that improved the interpretive discussion. This work was sponsored by the Galileo Project and was performed at the Jet Propulsion Laboratory, California Institute of Technology, under contract with NASA. G.S. and W.B.M. acknowledge support by grants from NASA through the Galileo Project at JPL and the Planetary Geology and Geophysics program.

24 February 1998; accepted 14 May 1998

Detection of Atomic Deuterium in the Upper Atmosphere of Mars

Vladimir A. Krasnopolsky,* Michael J. Mumma, G. Randall Gladstone

High-resolution spectroscopy of Mars' atmosphere with the Hubble Space Telescope revealed the deuterium Lyman α line at an intensity of 23 $\pm$ 6 rayleighs. This measured intensity corresponds to $HD/H_2 = 1.5 \pm 0.6 \times 10^{-4}$, which is smaller by a factor of 11 than HDO/H_2O. This indicates that fractionation of HD/H_2 relative to that of HDO/H_2O is not kinetically controlled by the rates of formation and destruction of H_2 and HD but is thermodynamically controlled by the isotope exchange $HD + H_2O \leftrightarrow HDO + H_2$. Molecular hydrogen is strongly depleted in deuterium relative to water on Mars because of the very long lifetime of H_2 (1200 years). The derived isotope fractionation corresponds to an estimate of a planetwide reservoir of water ice about 5 meters thick that is exchangeable with the atmosphere.

Dissociation of water vapor with subsequent escape of H, H_2, and O is the primary mechanism of water loss from Mars. It is believed that Earth, Venus, and Mars were formed by the same rocky and icy planetesimals (*1*), which resembled meteorites and comets in their composition, respectively. These planets are thus expected to have initially had the same chemical and isotope composition. If the mass of the terrestrial ocean (having a global-equivalent depth of 2.7 km) is scaled by the planetary mass ratio, the expected initial water abundance on Mars is a layer about 1 km thick, assuming that this layer covers the entire martian surface. Geological estimates (*2*, *3*) favor 300 to 500 m of water ice. The current estimated rate of water loss of 1.2 m per billion years (*4*–*6*) would not significantly affect this reservoir. However, the rate of escape of H, H_2, and O could have been much higher on early Mars (*7*), and a feature that should reflect the integrated loss of martian water is the D/H ratio. The measured D/H ratio in Mars' water vapor exceeds that of terrestrial water by a factor of 5.5 and corresponds to $HDO/H_2O = 1.7 \times 10^{-3}$ (*8*, *9*). It is generally believed that enrichments in heavy isotopes are mostly due to the preferential escape of light isotopes. The enrichment is especially strong for D because D is twice as massive as H.

D/H ratios measured in martian meteorites vary from 1.9 to 5.4 times Earth's ratio (*10*). These meteorites are thought to have been ejected from Mars by impact. High D/H ratios in martian crustal water (represented by D/H measured in martian mete-

V. A. Krasnopolsky, Department of Physics, Catholic University of America, Washington, DC 20064, USA, and NASA Goddard Space Flight Center (GSFC), Greenbelt, MD 20771, USA.
M. J. Mumma, NASA GSFC, Greenbelt, MD 20771, USA.
G. R. Gladstone, Southwest Research Institute, San Antonio, TX 78228, USA.

*To whom correspondence should be addressed at NASA/GSFC, Code 690.2, Greenbelt, MD 20771, USA. E-mail VKras@lepvx3.gsfc.nasa.gov

orites) imply a rather vigorous exchange between atmospheric water and deep water reservoirs on Mars, probably due to hydrothermal systems (*11*) associated with volcanism or with large impact craters. The martian meteorite results thus also suggest a high escape rate of water on early Mars (*7*).

The D enrichment in escape processes can be quantified by a fractionation factor

$$F = 2\,\frac{\phi_D/\phi_H}{HDO/H_2O} \qquad (1)$$

Here ϕ_D and ϕ_H are the escape rates for D and H, respectively. Model calculations yield $F = 0.32$ for Mars (*12*). A more direct way to get F is to measure the abundance of atomic D in Mars' upper atmosphere. This is the objective of our Hubble Space Telescope (HST) measurements.

The strongest spectroscopic feature of atomic H is the Lyman α line (Ly α) at wavelength $\lambda = 1215.670$ Å (*13*). The D Ly α line at 1215.338 Å (*14*) is weaker than the H line by more than two orders of magnitude. The Goddard high-resolution spectrograph (GHRS) onboard the HST (*15*) provided high sensitivity to detect the D line and high resolving power to separate the D line from the H line.

An attempt to detect D on Mars with GHRS was made before the HST scientific program began in 1991 (*16*), but no D emission was detected, with a 2σ upper limit of 30 rayleighs (R) (*17*). However, we found two ways to improve the detection conditions: (i) to observe Mars' limb instead of the illuminated disk center, and (ii) to observe at solar minimum instead of solar maximum. With the GHRS field of view 1.74″ × 1.74″, the expected signal increase is 2.5 for the limb observation of D. Our photochemical models (*6*) predict an increase in the H column abundance at solar minimum by a factor of 7 relative to solar maximum. However, the intensity of the solar line at 1216 Å is weaker by a factor of 3 at solar minimum, so that the net gain expected from the solar cycle conditions is 2.2. The total gain from both factors is 5.5.

We observed Mars on 20–21 January 1997 (*18*). A total of 36 spectra with 2000 sampling intervals in the range of 1212 to 1218 Å were acquired, each representing 435 s of integration. The charged-particle background varied from spectrum to spectrum (Figs. 1 and 2). The strongest emission was from foreground geocoronal H Ly α. Twenty spectra were measured in Earth's shadow, and subtraction of these spectra from those on the illuminated parts of the HST orbit allows us to establish the accurate position and shape of the geocoronal H emission. The expected emission of interplanetary hydrogen is small (*19*) (Fig. 1). Subtraction of the geocoronal and interplanetary H lines from the spectrum shows the martian H line with an intensity of 3.3 kR. The geocoronal and martian lines have half widths of 0.077 Å, which agree with the instrument resolving power of 1.6×10^4 (*20*). The position of the martian line agrees with the expected blue shift due to the geocentric velocity of Mars. One spectrum was measured on Mars' disk at 2000 km from the disk center; the observed H Ly α intensity was 3.3 ± 0.15 kR.

The measured spectrum (Fig. 2) reveals a feature between 1215.27 and 1215.38 Å with intensity of 47 ± 7 R. Its wavelength, width, and structure in the four-pixel binning suggest the presence of two components with almost equal intensities centered at 1215.295 and 1215.34 Å. The latter is the telluric D line. The martian D line should be at 1215.28 Å. However, the peak brightness is expected at 130 km above the limb (see below), and this increases the wavelength by 0.012 Å, which is close to the detected wavelength. Both martian and telluric D lines have intensities of 23 ± 6 R (*21*).

We observed Mars at the cold conditions of aphelion at solar minimum, which are similar to those experienced by the Viking entry probes (*22*). Thermal escape of D and HD was negligible at the expected temperature $T = 180$ K. The detection and analysis of He on Mars (*23*) showed the importance of nonthermal escape, which was ignored in previous models for H, H_2, D, and HD. We consider three processes contributing to the nonthermal escape of these species: (i) charge exchange with solar wind protons (*24*), (ii) electron impact ionization and dissociation (*25*), and (iii) photoionization (*26*). All of these escape processes occur above the ionopause where the product ions are swept away by the solar wind. Nonthermal escape dominates in the losses of D and H_2 at solar minimum and of HD under all conditions (Table 1).

To simulate the measurement, we calculated a photochemical model for D and HD

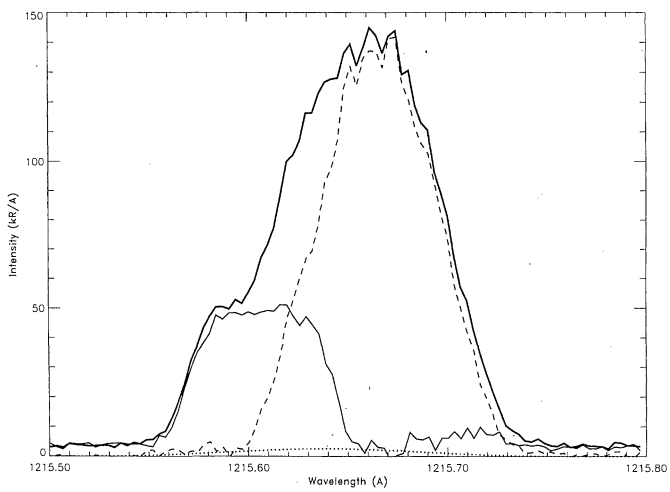

Fig. 1. Fragment of the HST spectrum (thick solid line) near the H Ly α line of the martian upper atmosphere. Geocoronal H (dashed line) and interplanetary H (dotted line) emissions are also shown. Their subtraction results in the martian hydrogen line (thin solid line). The geocoronal line is the difference of spectra recorded in the illuminated and shaded parts of the HST orbit.

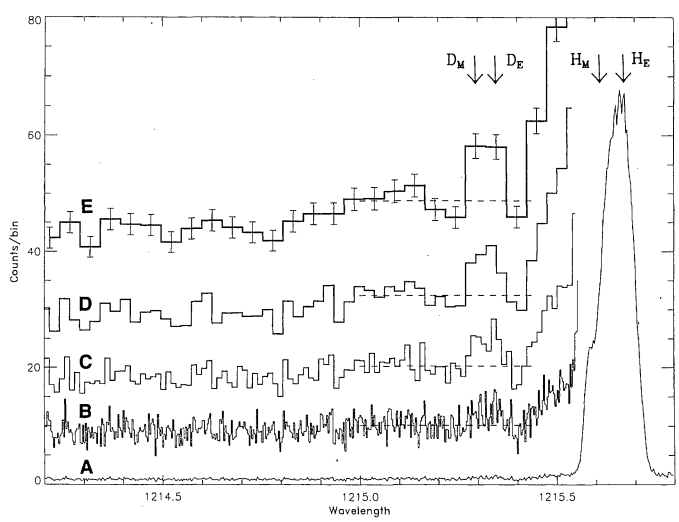

Fig. 2. Fragment of the HST spectrum that shows the martian and telluric D Ly α lines at 1215.29 and 1215.34 Å, respectively. A is the initial weighted mean spectrum, B is that spectrum scaled by a factor of 10, C is binned to 4 pixels and scaled by a factor of 5, D is binned to 8 pixels and scaled by a factor of 4, and E is binned to 16 pixels and scaled by a factor of 3. Dashed horizontal lines indicate the local background baselines. The positions of the martian and telluric D and H lines are shown; subscript M and E refer to Mars and Earth, respectively.

from 80 to 250 km altitude in the martian atmosphere. HD forms D in reactions with CO_2^+, O^+, and $O(^1D)$ (*27*, *28*). The model corresponds to global-mean conditions and has the HD density at 80 km as a parameter (*29*). Then we applied a radiative transfer code for a spherical atmosphere, which accounts for single scattering and self-absorption by D atoms and absorption by CO_2 (*30*). With the known shape and intensity of the solar H Ly α line (*31*), we calculated an emission rate factor $g_D = 3.5 \times 10^{-4}$ photons per second per atom for 1.67 astronomical units (AU) at solar minimum. Applying our code to the profiles of D density calculated with our photochemical model (Figs. 3 and 4), we find that, to fit the measured intensity for the D Ly α line of 23 ± 6 R, the HD density should be equal to $1.6 \pm 0.5 \times 10^5$ cm^{-3} at 80 km, and its mixing ratio is 6 ± 2 parts per billion (ppb). The lifetimes of H_2 and HD are 1200 years in the martian atmosphere (*5*), and their mixing ratios should be constant up to the homopause (≈110 km) and should not vary from place to place and in time intervals less than a few hundred years.

Now we need to compare the HD mixing ratio with that of H_2. Like HD, the H_2 mixing ratio may be obtained from measurements of the H Ly α line, radiative transfer analysis (which must include multiple scattering), and photochemical modeling. We allocated one HST orbit for measurements of H Ly α at three points above Mars' limb. However, these observations were not made, owing to operational difficulties. We can deduce H_2 from the measured H Ly α limb intensity of 3.3 kR, but the result would be sensitive to small errors in the instrument calibration and in the adopted intensity at the center of the solar H Ly α line. Therefore, we used the Mariner 6 and 7 measurements (*4*). According to those measurements, which were made near solar maximum, [H] = 2.5 to 3×10^4 cm^{-3} at 250 km, $T \approx 350$ K, and the optical depth of atomic H was ≈2.2. Our photochemical model for H and H_2 (Fig. 3) (*32*) is similar to that for D and HD and the model in (*4*). An H_2 mixing ratio of 40 ± 10 parts per million (ppm) reproduces both the H density at 250 km and the optical depth in our model. The H_2 mixing ratio exceeds 20 ppm obtained in (*4*) but agrees with models involving the photochemistry of many species (*5*), which give 35 to 50 ppm for H_2.

We conclude that $HD/H_2 = 1.5 \pm 0.6 \times 10^{-4}$ (*33*) and enrichment R of D in H_2 relative to H_2O is

$$R = \frac{HD/H_2}{HDO/H_2O} = 0.09 \pm 0.04 \quad (2)$$

This value is smaller than $R = 1.6$ calculated in (*12*) under an assumption that partitioning of D between HD and HDO is kinetically controlled by reactions of formation and removal of HD. If, however, the isotope exchange is controlled thermodynamically in collisions between H_2O and H_2 molecules

$$HD + H_2O \leftrightarrow HDO + H_2 \quad (3)$$

then $R = 0.14 \pm 0.06$ is expected at $T = 200 \pm 20$ K (*12*, *34*), which agrees with our measurement. This means that although freshly formed H_2 is enriched in D relative to H_2O on Mars by the kinetic factor of $R = 1.6$, during its lifetime of 1200 years it tends to lose D in collisions with H_2O, and the lifetime-mean value of R is 0.09 ± 0.04. The lifetime of HD relative to the isotope exchange $HD + H_2O$ must thus be at least a factor of 10 shorter than 1200 years. This imposes a constraint on the isotope exchange rate coefficient (*35*)

$$k_{HD+H_2O} \geq 10^{-23} \text{ cm}^3 \text{ s}^{-1} \quad (4)$$

The next step is calculation of the fractionation factor F. Data from Table 1 and Fig. 3 result in $\phi_D/\phi_H = 1.9 \times 10^{-5}$ and 1.8×10^{-5} for solar minimum and maximum, respectively. Similar modeling for mean solar activity gives 1.4×10^{-5}. The resulting

Table 1. Dayside escape frequencies above the ionopause and global mean effusion velocities for escape processes of H, D, H_2, and HD on Mars. Nonthermal escape should vary with solar activity. However, we do not have enough input data to calculate those variations and instead use the constant values.

Process	H	D	H_2	HD
Charge transfer with protons (10^{-8} s^{-1})	26	26	5	5
Electron impact (10^{-8} s^{-1})	15	15	25	25
Photoionization (10^{-8} s^{-1})	3.2	3.2	3.7	3.7
V_n* (cm s^{-1})	21	8	6.4	3.7
V_t 180 K† (cm s^{-1})	165	0.08	0.08	4×10^{-5}
V_t 200 K‡ (cm s^{-1})	350	0.39	0.39	4×10^{-4}
V_t 280 K§ (cm s^{-1})	2340	19	19	0.145
V_t 350 K‖ (cm s^{-1})	6000	133	133	2.74

*V_n is total nonthermal escape velocity calculated for the ionopause at 300 km. V_t is thermal escape velocity for †aphelion at solar minimum, ‡solar minimum, §solar mean, and ‖solar maximum.

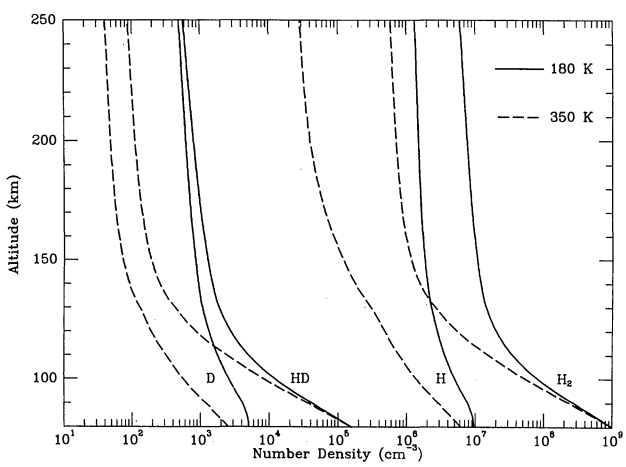

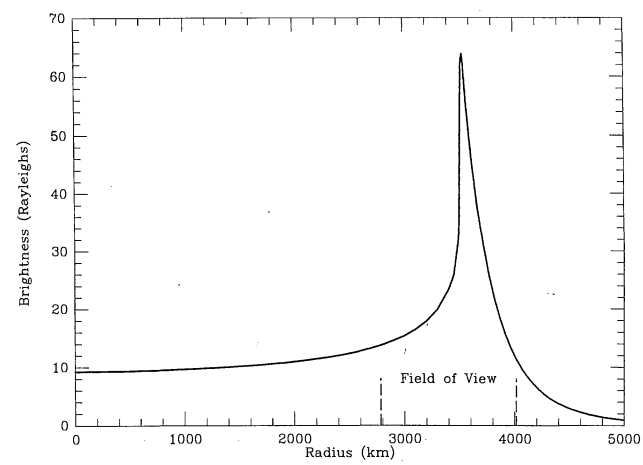

Fig. 3 (left). Calculated H_2, H, HD, and D densities for the conditions of the HST observations (aphelion, solar minimum, $T = 180$ K) and Mariner 6 and 7 observations (solar maximum, $T = 350$ K). **Fig. 4 (right).** Calculated brightness of the D line versus radius. The HST field of view is centered on the limb, and the measured brightness of 23 R exceeds that in the disc center by a factor of 2.5. The brightness maximum at 130 km above the limb results in a small wavelength shift in the observed emission.

fractionation factor is $F = 0.02$ for the average escape flux ratio, which is much smaller than the value of 0.32 calculated in (*12*).

Liquid water could exist on Mars up to the end of the erosion of the atmosphere by large-scale meteorite impacts (*36*) at 0.8 billion years after the planet formed. This erosion reduced the initial CO_2 abundance of 7.5 bars (*1*) by a factor of 100. Water was less affected by impact erosion than CO_2, and impact erosion could not change the D/H ratio. Further escape of H_2O is estimated at $a_e \approx 30$ m (*a*, abundance of water; e, escape) (*7*). We can apply the derived *F* to a model of H_2O escape and D fractionation after the end of impact erosion. We assume that the bulk H_2O reservoir has the terrestrial D/H ratio. The second reservoir is in isotope equilibrium with the atmospheric H_2O vapor, which is the third reservoir. Deuterium in H_2O vapor may be depleted relative to its abundance in H_2O ice by a factor of 0.79 (*12*, *37*, *38*). This model shows (*39*) that the reservoir that is exchangeable with the atmosphere is $a \approx 0.17a_e \approx 5$ m thick; that is, about 1% of the current water abundance (*2*, *3*) and about the size of the exchangeable reservoir in the polar caps (*2*, *40*). Acuna *et al.* (*41*) infer the existence of an intrinsic magnetic field on early Mars. This field should reduce escape processes in that epoch and favors a smaller value of a_e (*42*). However, $a \approx 0.17a_e$ still holds.

Our results show that H_2 is depleted in D relative to water on Mars. This depletion occurs because of the long lifetime of H_2 on Mars. H_2 is the intermediate species that forms H in the upper atmosphere, and the depletion of H_2 in D results in the low abundance and escape of atomic D. On Venus, by comparison, H_2 is a minor source of H (*41*) and cannot affect the abundance of atomic D.

REFERENCES AND NOTES

1. T. Owen and A. Bar-Nun, *Icarus* **116**, 215 (1995). However, D in comets is enriched relative to Earth's value [P. Eberhardt, M. Reber, D. Krankovsky, R. R. Hodges, *Astron. Astrophys.* **302**, 301 (1995)].
2. M. H. Carr, *Icarus* **87**, 210 (1990); D. M. Hunten, *Science* **259**, 915 (1993).
3. T. M. Donahue, *Nature* **374**, 432 (1995).
4. D. E. Anderson, *J. Geophys. Res.* **79**, 1513 (1974).
5. V. A. Krasnopolsky, *Icarus* **101**, 313 (1993); H. Nair, M. Allen, A. D. Anbar, Y. L. Yung, R. T. Clancy, *ibid.* **111**, 124 (1994); V. A. Krasnopolsky, *J. Geophys. Res.* **100**, 3263 (1995).
6. V. A. Krasnopolsky, *Icarus* **101**, 33 (1993).
7. Total losses of 30 m of H_2O and 40 mbar of CO_2 since the end of impact erosion have been calculated by B. M. Jakosky, R. O. Pepin, R. E. Johnson, and J. L. Fox [*Icarus* **111**, 271 (1994)], based on the data of J. G. Luhmann, R. E. Johnson, and M. H. G. Zhang [*Geophys. Res. Lett.* **19**, 2151 (1992)]. Other calculations of the H_2O and CO_2 losses are more affected by some questionable assumptions.
8. $HDO/H_2O = 2$ D/H, and the terrestrial ratio is D/H = 1.56×10^{-4} [R. Hagemann, G. Nief, E. Roth, *Tellus* **22**, 712 (1970)] in standard mean ocean water.
9. T. Owen, J. P. Maillard, C. de Bergh, B. L. Lutz, *Science* **240**, 1767 (1988); V. A. Krasnopolsky, G. L. Bjoraker, M. J. Mumma, D. E. Jennings, *J. Geophys. Res.* **102**, 6525 (1997). The abstract of G. L. Bjoraker, M. J. Mumma, and H. P. Larson [*Bull. Am. Astron. Soc.* **21**, 991 (1989)] is under revision.
10. L. L. Watson, I. D. Hutcheon, S. Epstein, E. Stolper, *Science* **265**, 86 (1994).
11. B. M. Jakosky and J. H. Jones, *Nature* **370**, 328 (1994).
12. Y. L. Yung *et al.*, *Icarus* **76**, 146 (1988).
13. This line consists of two components at 1215.668 and 1215.674 Å, with the intensity ratio of 2:1. The weighted mean wavelength is 1215.670 Å.
14. The isotope shift is given by
$$\Delta\lambda = \lambda m \left(\frac{1}{M_H} - \frac{1}{M_D}\right) = 0.332\text{Å}$$
Here *m*, M_H, and M_D are the masses of the electron, H, and D, respectively.
15. GHRS was replaced with the Space Telescope imaging spectrograph (STIS) in February 1997. Although STIS has many advantages when compared with GHRS, its dark current per square arc second is higher than that of GHRS by a factor of 8, and exposures required to detect weak emissions from extended sources are longer by the same factor.
16. J. L. Bertaux, J. T. Clarke, M. Mumma, T. Owen, E. Quemerais, in *Science with the Hubble Space Telescope*, P. Benvenuti and E. Schreier, Eds. (European Southern Observatory, Garching, Germany, 1992), p. 459; J. T. Clarke, R. Lallement, J. L. Bertaux, E. Quemerais, *Astrophys. J.* **448**, 893 (1995).
17. One R corresponds to a column production of 10^6 photons cm^{-2} s^{-1} $(4\pi$ ster$)^{-1}$.
18. The heliocentric and geocentric distances of Mars were 1.67 and 0.97 AU, respectively, and the geocentric velocity was −15.4 km s^{-1}. Observations were done during eight HST orbits with a total exposure of 1.6×10^4 s. The instrument field of view was 1230×1230 km^2, centered on the bright limb. The solar activity index was $F_{10.7\ cm} = 70$.
19. The angle between the instrument direction and the velocity of the interstellar wind was 115°, therefore the line of interplanetary H was Doppler shifted by −0.052 Å and its Doppler width was 0.06 Å [F. M. Wu and D. L. Judge, *Astrophys. J.* **239**, 389 (1980)]. The line intensity was 200 R for this direction at solar minimum [J. M. Ajello, A. I. Stewart, G. E. Thomas, A. Graps, *ibid.* **317**, 964 (1987)]. Half of the field of view was screened by Mars, reducing the effective intensity to 100 R and modifying the wavelength shift to −0.026 Å.
20. The GHRS resolving power was 10^5 for an aperture of 0.22″ × 0.22″ and smaller by a factor of 6 for 1.74″ × 1.74″. The difference in sensitivities for these apertures was a factor of 64.
21. Both D lines binned in 16 pixels result in signal-to-noise ratios of 5. The given uncertainty accounts for both statistical and baseline uncertainties.
22. A. O. Nier and M. B. McElroy, *J. Geophys. Res.* **82**, 4341 (1977).
23. V. A. Krasnopolsky, S. Bowyer, S. Chakrabarti, G. R. Gladstone, J. S. McDonald, *Icarus* **109**, 337 (1994); V. A. Krasnopolsky and G. R. Gladstone, *J. Geophys. Res.* **101**, 15765 (1996).
24. Cross sections are 2×10^{-15} cm^2 for H and D [J. H. Newman *et al.*, *Phys Rev. A* **25**, 2976 (1982)] and 4×10^{-16} cm^2 for H_2 and HD [Y. Nakai *et al.*, *At. Data Nucl. Data Tables* **37**, 69 (1987)]. The typical solar wind proton flow is 1.3×10^8 cm^{-2} s^{-1} at Mars' orbit.
25. Densities and energies of electrons above Mars' ionopause are from M. H. G. Zhang, J. G. Luhmann, A. F. Nagy, J. P. Spreiter, and S. S. Stahara [*J. Geophys. Res.* **98**, 3311 (1993)]. Cross sections are from L. J. Kieffer [*At. Data* **1**, 19 (1969)].
26. Solar photon fluxes are from P. G. Richards, J. A. Fennelly, and D. G. Torr [*J. Geophys. Res.* **99**, 8981 (1994)]. Cross sections are from S. K. Atreya [*Atmospheres and Ionospheres of the Outer Planets and Their Satellites* (Springer, New York, 1986)].
27. Those reactions are as follows: (i) net HD + CO_2^+ (+ e) → CO_2 + H + D; $k_1 = 5.6 \times 10^{-10}$ cm^3 s^{-1}. (ii) net HD + O^+ (+ e) → O + H + D; $k_2 = 1.22 \times 10^{-9}$ cm^3 s^{-1}. (iii) net HD + $O(^1D)$ (+ O) → O_2 + H + D; $k_3 = 10^{-10}$ cm^3 s^{-1}. k_1 is the mean of those for H_2 and D_2 from V. G. Anicich, *J. Phys. Chem. Ref. Data* **22**, 1469 (1993); k_2 is from the same paper; k_3 is from W. B. DeMore *et al.*, *JPL Publ. 94-26* (1994).
28. Atomic H and D are formed by H_2O photolysis in the lower atmosphere. H_2O does not directly participate in formation of atomic H and D in the upper atmosphere. Because of the long lifetime of H_2 (which forms H and D in the upper atmosphere), the abundances of H and D in the upper atmosphere are insensitive to strong variations of H_2O vapor in the lower atmosphere.
29. The transport time $t = H^2/(K + D_i)$ is longer than 1 day throughout most of the altitude range, therefore the HD and D density profiles are better reproduced by assuming global mean conditions than using local conditions. Here *H* is the species scale height, and *K* and D_i are the eddy and molecular diffusion coefficients taken from (*6*). Molecular diffusion coefficients for D and HD are smaller than those for H and H_2 by factors of $2^{1/2}$ and $1.5^{1/2}$, respectively. The CO_2^+ and O^+ densities were taken from the Viking measurements [W. B. Hanson, S. Santanini, D. R. Zuccaro, *J. Geophys. Res.* **82**, 4351 (1977)] and corrected for the global mean conditions by a factor of $(4 \cos 42°)^{-1} = 0.336$. The $O(^1D)$ density was calculated. The upper boundary conditions are the escape velocities from Table 1; the condition for D at the lower boundary is velocity $V = -K/H$.
30. The Ly α scattering cross section of D is 6×10^{-12} $T^{-1/2}$ cm^2 at the line center, and the Ly α absorption cross section of CO_2 is 7.5×10^{-20} cm^2. Self-absorption by D atoms is only a few percent, confirming the validity of the single scattering approximation.
31. P. Lemaire *et al.*, *Astrophys. J.* **223**, L55 (1978).
32. $k_1 = 6.2 \times 10^{-10}$ cm^3 s^{-1}, $k_2 = 1.6 \times 10^{-9}$ cm^3 s^{-1}, and $k_3 = 10^{-10}$ cm^3 s^{-1} for the reactions of H_2, which are similar to those of HD in (*27*) and taken from the same sources. As for HD, the model reflects the global mean conditions but for solar maximum. These differ from the daytime conditions of the model in (*4*). Temperature, ion density, and eddy diffusion profiles are taken from the solar maximum model in (*6*).
33. We assume uncertainties associated with modeling of HD and H_2 to be 25%. Because of the similarity of the models for HD and H_2, these uncertainties cancel out in HD/H_2.
34. This value and its uncertainty were calculated using data from L. V. Gurvich, I. V. Veyts, and C. B. Alcock [*Thermodynamic Properties of Individual Substances*, Hemisphere Publishing, New York, 1989)]. The uncertainties of the given temperature and the thermodynamic constants contribute equally to the final value.
35. The D exchange rate coefficient may be calculated as
$$k_{HD + H_2O} = \frac{\int_0^\infty [H_2]dz}{\tau \int_0^\infty [H_2][H_2O]dz} \quad (5)$$
where $\tau \leq 120$ years, given in seconds, and the water abundance is 10 precipitated micrometers uniformly mixed up to 15 km. The obtained value of k_{HD+H_2O} is larger than that measured in the laboratory [C. Lecluse and F. Robert, *Geochim. Cosmochim. Acta* **58**, 2927 (1994)]. See discussion in Y. L. Yung and D. M. Kass, *Science* **280**, 1545 (1998).
36. H. J. Melosh and A. M. Vickery, *Nature* **338**, 487 (1989).
37. This factor depends on temperature and is equal to 0.79 ± 0.05 for $T = 220 \pm 20$ K [L. Merlivat and G. Nief, *Tellus* **19**, 122 (1967)].
38. Diurnal and seasonal condensation and sublimation occur without fractionation between ice and vapor. For example, seasonal polar caps sublime completely without fractionation and may be considered as a part of reservoir three. We assume that fractionation exists between reservoirs two and three because the exchange of H_2O between them is slow and reservoirs do not completely disappear. This

assumption is questionable.
39. The abundance of water a in reservoir two does not vary in this model. Integration of the appropriate differential equation results in

$$\frac{(D/H)_{Mars}}{(D/H)_{Earth}} = \frac{1}{f} - \left(\frac{1}{f} - 1\right)e^{-\frac{a_e}{a}f} \quad (6)$$

for constant escape flux and a more complicated expression for variable flux; $f = 0.79F$. However, the result is rather insensitive to the adopted temporal dependence of escape flux. Our calculation was made for $\phi(t) = 25\ e^{-t/\tau}$ m per billion years, where $\tau = 1.25$ billion years (Gyr). This relation fits the current escape flux of 1.2 m Gyr^{-1} and the total escape $a_e = 30$ m. Our model differs from the model (*12*) in which reservoir two is disconnected from reservoir one and gradually shrinks from 3.6 to 0.2 m.
40. Reservoir two may be a part of the polar cap water, which is estimated at 15 m by B. M. Jakosky [*J. Geophys. Res.* **95**, 1475 (1990)]. It should also include some crustal water.
41. M. H. Acuna *et al.*, *Science* **279**, 1676 (1998).
42. W. Stumpner, H. Lammer, S. J. Bauer, *Ann. Geophys.* **16** (suppl. 111) C1002 (1998).
43. See figure 184 in V. A. Krasnopolsky, *Photochemistry of the Atmospheres of Mars and Venus* (Springer, New York, 1986).
44. V.A.K. thanks T. Reyes for consulting in data processing. This work was supported by the HST Guest Observer Program.

23 January 1998; accepted 6 April 1998

Atmosphere-Surface Interactions on Mars: $\Delta^{17}O$ Measurements of Carbonate from ALH 84001

James Farquhar, Mark H. Thiemens, Teresa Jackson

Oxygen isotope measurements of carbonate from martian meteorite ALH 84001 ($\delta^{18}O$ = 18.3 ± 0.4 per mil, $\delta^{17}O$ = 10.3 ± 0.2 per mil, and $\Delta^{17}O$ = 0.8 ± 0.05 per mil) are fractionated with respect to those of silicate minerals. These measurements support the existence of two oxygen isotope reservoirs (the atmosphere and the silicate planet) on Mars at the time of carbonate growth. The cause of the atmospheric oxygen isotope anomaly may be exchange between CO_2 and $O(^1D)$ produced by the photodecomposition of ozone. Atmospheric oxygen isotope compositions may be transferred to carbonate minerals by CO_2-H_2O exchange and mineral growth. A sink of ^{17}O-depleted oxygen, as required by mass balance, may exist in the planetary regolith.

Chemical and isotopic measurements of the present-day martian atmosphere indicate that many elements and isotopes are fractionated from their initial compositions (*1*). Modeling suggests that the composition of the martian atmosphere has evolved on planetary time scales as a result of escape processes, impact erosion, outgassing, and photochemical reactions (*2–6*). Morphologic evidence points to times early in martian history when greenhouse heating supported warmer climates and liquid water shaped Mars's surface (*7, 8*). Measurements of trapped gases and mineral phases in martian meteorites indicate that atmospheric evolution occurred before the excavation of these meteorites from the martian surface (*9–15*).

The present martian atmosphere interacts with the hydrosphere and regolith through diurnal, seasonal, and longer term exchange of water between the atmosphere and regolith (*16, 17*). In the past, liquid water acted as a medium for atmosphere-surface exchange and new mineral precipitation. High rates of oxygen exchange between H_2O and CO_2 facilitated the transfer of atmospheric oxygen isotopic characteristics to H_2O and to minerals that precipitated from it. Because oxygen is present in CO_2, H_2O, dust, and other atmospheric constituents such as O_2, CO, and O_3, the oxygen isotope compositions of minerals formed in the regolith serves as a tracer for atmospheric chemistry and evolution and its interactions with the martian surface. Here we report measurements (*18*) of ^{16}O, ^{17}O, and ^{18}O in carbonate minerals from martian meteorite ALH 84001 [$\delta^{18}O$ = 18.3 ± 0.4‰, $\delta^{17}O$ = 10.3 ± 0.2‰, and $\Delta^{17}O$ = 0.8 ± 0.05‰ (*23*)]. High-temperature silicate phases in ALH 84001 give $\delta^{18}O$ = 4.53 to 4.64‰, $\delta^{17}O$ = 2.58 to 2.74‰, and $\Delta^{17}O$ = 0.22 to 0.327‰ (*12*). Secondary ion mass spectrometry analysis of SiO_2 yielded $\delta^{18}O$ = 20.4 ± 0.9‰ (*24*), and analyses of carbonate have yielded $\delta^{18}O$ = –9 to 26‰. The mean of these measurements is 15 ± 5‰ (one 3σ outlier is omitted) (*15, 24–26*). Our $\delta^{18}O$ measurements fall within the range of previous measurements for carbonates but differ from the $\Delta^{17}O$ of the high-temperature silicate phases.

Karlsson *et al.* (*27*) extracted H_2O from six martian meteorites by stepwise pyrolysis and found that the $\Delta^{17}O$ of this water ranged from 0.1 to 0.9‰. H_2O extracted from Nakhla, Lafayette, Chassigny, and Zagami meteorites during 600° and 1000°C pyrolysis steps ($\Delta^{17}O$ = 0.4 to 0.9‰) was fractionated relative to martian meteorite silicates [$\Delta^{17}O$ ~ 0.3‰ (*12*)]. The same pyrolysis steps for Shergotty produced H_2O unfractionated with respect to martian meteorite silicates, and for meteorite EETA 79001 they produced H_2O with $\Delta^{17}O$ = 0.1‰, which is intermediate between terrestrial waters ($\Delta^{17}O$ = 0) (*11*) and martian meteorite silicates. These results (*27*) were interpreted to indicate that H_2O extracted from Nakhla, Lafayette, Chassigny, Zagami, and Shergotty had a martian origin and that H_2O extracted from EETA 79001 was a mixture of martian and terrestrial waters. Because water extracted from Nakhla, Lafayette, Chassigny, and Zagami was not in oxygen isotopic equilibrium with martian meteorite silicate minerals, two distinct oxygen reservoirs were inferred to be present on Mars—the silicate planet (the crust and mantle) and the atmosphere (including H_2O that exchanged oxygen with it).

Our measurements of carbonates ($\Delta^{17}O$ = 0.8‰) are fractionated relative to measurements of martian meteorite silicates and indicate that ALH 84001 also preserves evidence of oxygen isotope disequilibrium between the atmosphere and the silicate planet. Carbonate nodules in ALH 84001 preserve chemical and isotopic gradients (*24, 25, 28*) that would have been homogenized by diffusion and exchange if postgrowth reequilibration occurred. Our oxygen isotope data therefore indicate that the atmosphere and lithosphere were out of isotopic equilibrium at the time of carbonate growth.

On Earth, plate tectonics facilitates oxygen exchange between the hydrosphere and lithosphere through global-scale hydrothermal circulation systems at plate margins. Because the amount of oxygen in the silicate Earth is greater than that in the hydrosphere and atmosphere, this exchange buffers the oxygen isotope composition of the hydrosphere (*29*). The oxygen isotope composition of water in Earth's oceans is buffered to a steady-state value on a time scale with a mean life (1/rate constant) of ~100 to 250 million years (*29*). The lack of plate tectonics on Mars is seen as a means of maintaining an atmosphere that is isotopically distinct from the solid planet (*27*). It is unclear whether other types of hydrothermal activity may have caused sufficient atmosphere-surface oxygen exchange to affect atmospheric $\delta^{18}O$, $\delta^{17}O$, and $\Delta^{17}O$. Massive hydrothermal systems have been invoked to explain surface features associated with the Oceanus Borealis and spectroscopic features in the Valles Marineris canyon system (*7, 30*) and also as a means of generating catastrophic floods and release of CO_2 of sufficient quantity to stabilize episodic, greenhouse-state, atmospheric conditions with higher CO_2 pressure (*7*). If these

Department of Chemistry, University of California San Diego, 92093–0356, USA. E-mail: jfarquha@ucsd.edu (J.F.), mht@ucsd.edu (M.H.T.), tjackson@ucsd.edu (T.J.)